INFLUENCE OF WIND DIRECTION ON THE SURFACE ROUGHNESS OF VINEYARDS

Joseph G. Alfieri[1], William P. Kustas[1], Hector Nieto[2], John H. Prueger[3], Lawrence E. Hipps[4], Lynn G. McKee[1], Feng Gao[1], Sebastian Los[4]

[1]USDA ARS, Hydrology and Remote Sensing Laboratory, Beltsville, MD 20705-2350 USA
[2]Institute for Food and Agricultural Research & Technology, Parc de Gardeny, Edifici Fruitcentre, 25003 Lleida, Spain
[3]USDA ARS, National Laboratory for Agriculture and the Environment, Ames, IA 50011 USA
[4]Plants, Soils and Climate Department, Utah State University, Logan, UT 84322-4820 USA

Corresponding author: Joseph G. Alfieri; joe.alfieri@ars.usda.gov

ABSTRACT

Remote sensing-based models are the most viable means of collecting the high-resolution spatially distributed estimates of evaporative water loss needed to manage irrigation and ensure the effective use of limited water resources. However, due to the unique canopy structure and configuration of vineyards, these models may not be able to adequately describe the physical processes driving evapotranspiration from vineyards. Using data collected from 2014 to 2016 as a part of the Grape Remote sensing Atmospheric Profile and Evapotranspiration Experiment (GRAPEX), the twofold objective of this study was to *i.* identify the relationship between the roughness parameters, zero-plane displacement height (d_o) and roughness length for momentum (z_o), and local environmental conditions, specifically wind direction and vegetation density and *ii.* determine the effect of using these relationships on the ability of the remote sensing-based Two-Source Energy Balance (TSEB) model to estimate the sensible (H) and latent (λE) heat fluxes. Although little variation in d_o was identified during the growing season, a well-defined sigmoidal relationship was observed between z_o and wind direction. When the output from a version of the TSEB model incorporating these relationships (TSEB$_{VIN}$) was compared to output from the standard model (TSEB$_{STD}$), there were large changes to the roughness parameters, particularly z_o, but only modest changes in the turbulent fluxes. When the output from TSEB$_{VIN}$

was compared to that of a version using a parameterization scheme representing open canopies ($TSEB_{OPN}$), the mean absolute difference between the estimates of d_o and z_o were 0.44 m and 0.25 m, respectively. While these values represent differences in excess of 45%, the turbulent fluxes differed by just 13 W m^{-2} or 10%, on average. The results suggest that the TSEB model is largely insensitive to changes in the roughness parameters. This also suggests that the requirement for highly accurate roughness values has limited utility in the application of the TSEB model in vineyard systems. Since there is no significant advantage to using the more complex $TSEB_{OPN}$ and $TSEB_{VIN}$ models, it is recommended that the standard model be used.

INTRODUCTION

In terms of both quantity and value, California is among the largest wine producing regions in the world. According to statistics compiled by the US Department of the Treasury (2017), California's average wine production during the last decade approaches 2.41 GL (638 million gallons) of wine annually; this is nearly 90% of all US production. As a result, the California wine industry contributes nearly $60B to the state's economy and $115B to the US economy each year according to industry analyses (MKF Research, 2007; John Dunham and Associates, 2016). In turn, the wine industry is dependent on the state's wine grape growers. There are approximately 250,000 ha of wine grape vineyards in California producing 363 Gg of fruit valued at more than $3B each year (California Department of Food and Agriculture, 2017).

Since California, like many other wine-producing regions, is characterized by limited rainfall and high evaporative demand during the growing season, irrigation is critical to ensure vineyard productivity. However, the timing and amount of water available can significantly impact the vine vigor, crop yield, and fruit quality (Chapman et al. 2005; Chaves et al. 2007; Webb et al. 2007). For example, while adequate moisture is needed early in the growing season from bud burst to fruit set to ensure crop yield, moderate water stress is preferred later in the growing season to enhance fruit quality (Lobell et al. 2007; Zarrouk et al. 2012). Therefore, careful irrigation management is of paramount importance to wine grape production (Ojeda et al. 2002; Pellegrino et al. 2005; Acevedo-Opazo et al. 2010; Bellvert et al. 2015). Moreover, the factors influencing water availability, water loss via evapotranspiration, and crop water stress are numerous and vary both spatially and temporally. Thus, as discussed by Arno et al. (2009), Campos et al. (2010), and Pagay (2016), among others, precision methods for scheduling irrigation at a sub-vineyard scale are needed so that both the timing and amount of water applied to the vines is appropriate to their individual needs.

Remote sensing-based approaches are the most viable means to monitor the within-field variability in water loss and vine water stress needed for irrigation management decisions (Baluja et al. 2012; Semmens et al. 2016; Xia et al. 2016). However, remote sensing-based models also have limitations. One of these limitations is the simple empirical relations that are typically used to determine the parameters that describe the aerodynamic roughness of the surface which are used not only to calculate the wind profiles but also the resistance terms needed to calculate the fluxes of heat and moisture. For instance, the thermal remote sensing-based two-source energy balance model (TSEB; Norman et al.1995; Kustas and Norman1997, 1999, 2000), and the closely related ALEXI/DisALEXI modeling system (Anderson et al., 1997, 2004, 2007), determine two key roughness parameters, namely the zero-plane displacement height (d_o; referred to as displacement height hereafter) and roughness length for momentum (z_o; referred to as roughness length hereafter) as a fraction of vegetation height following the well-known relationships given by Norman and Campbell (1980).

The surface roughness parameters, d_o and z_o, describe the effect exerted by the surface on near-surface wind flow due to drag. They are often defined in terms of Monin-Obukhov Similarity Theory and the vertical profile of horizontal wind speed (Brutsaert 1982; Arya 2001). In this framework, z_o is defined as the height above the lower boundary of the logarithmic profile where the horizontal wind speed goes to zero. Depending on the size and density of the roughness elements, the position of the lower boundary lies somewhere between the base and top of the roughness elements. As the name implies, the d_o accounts for the height of the lower boundary of the profile above the land surface. However, these quantities can also be defined in terms of momentum transfer. In this context, z_o characterizes the efficiency of momentum transport to the surface (Shaw and Pereira 1982) while d_o indicates the mean height of momentum transfer to the surface (Raupach 1992, 1994; Brunett et al. 1994)

The commonly-used relationships between d_o, z_o and vegetation height, such as those used by TSEB and ALEXI/DisALEXI, neglect numerous other factors including the spacing, geometry, and frontal area that impact surface roughness by assuming dense closed canopy. (See Brutsaert (1982) for a concise discussion of the evolution of these empirical relationships.) In contrast, d_o and z_o for sparse or open canopies are also influenced by the organizational structure of the canopy, i.e. the density and distribution of biomass (Shaw and Pereira 1982; Raupach 1992, 1994; Verhoef et al. 1997). As discussed by Zeng and Wang (2007), failing to account for the factors beyond canopy height that can affect surface roughness, significant errors of up to 50% can be introduced into the estimates of d_o and z_o. Other studies, such as Pitman (1994) and Maurer et al. (2013, 2015) have shown errors in d_o and z_o can result in significant errors in modeled fluxes of momentum, heat, and moisture.

Although the exact configuration varies from vineyard-to-vineyard, vineyards are generally characterized by trellised vines that are between 1 m and 2.5 m in height and separated by a broad inter-row space on the order of 3 m wide. Due to this design, it is likely that d_o and z_o are influenced other factors beyond vine height. Although studies are limited, past research also suggests d_o and z_o are impacted by wind direction and vegetation density. The observational studies of Hicks (1973) and Riou et al. (1987) suggests surface roughness varies with wind direction while the work of Sene (1994) suggests that the surface roughness increases with increasing vine density. These results are further supported by the work of Weiss and Allen (1976), who found that turbulent intensity was greater when the wind flow was perpendicular to the vine rows as opposed to parallel to them, and Padro et al. (1994), who found that the aerodynamic resistance over a vineyard changed as a function of wind direction. Most recently, the large eddy simulation (LES) studies of Chahine et al. (2014) indicates that both d_o and z_o vary with wind direction with the lowest z_o and largest d_o occurring when winds are parallel to the rows.

Building on these earlier studies, the objective of this study was twofold. The first aim was to identify a functional relationship between each of the roughness parameters, d_o and z_o, and both wind direction and vegetation density as expressed in terms of leaf area index (LAI). The second objective was to evaluate the impact of allowing the roughness parameters to vary dynamically in response to changing environmental conditions on the surface fluxes computed by the TSEB model. The following section provides a description of field site, datasets, remote sensing-based ET model, and analysis techniques. The third section discusses the results of this study. Finally, the last section includes the conclusions and recommendations that can be drawn from this work.

MATERIALS AND METHODS

Site Description

As can be seen in Figure 1, the study was conducted as a part of the Grape Remote sensing Atmospheric Profile and Evapotranspiration eXperiment (GRAPEX) over a pair of adjacent vineyards located near the city of Lodi in California's Central Valley, USA (38.29 N 121.12 W). This region is characterized by warm, dry conditions and an evaporative demand ranging from 889 to 1270 mm of water during the growing season, which is defined here as April through August (Semmens et al. 2015). Also, the air temperature averages near 22°C and the total precipitation is typically 24 mm during the same period.

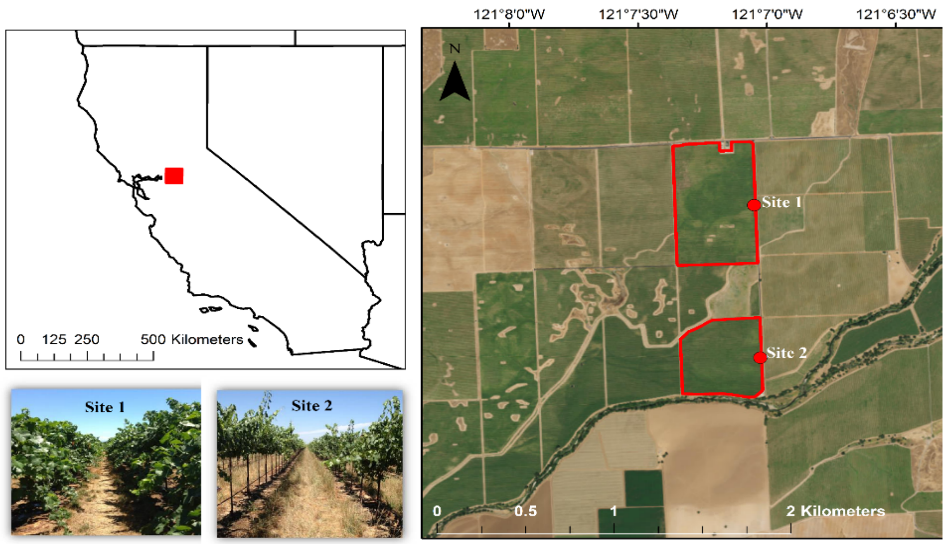

Figure 1 The location of study area is shown. The northern (Site 1) and southern (Site 2) vineyards are outlined in red while the location of the micrometeorological towers are represented by the red dots. The photo of the two vineyards were taken on August 6th, 2013.

Both vineyards are planted with Pinot Noir vines and share similar trellis structure and vine management. The main shoots of the vines, which are planted every 1.52 m along the east-west running trellising system, are attached to the quadrilateral cordon trellis at a height of 1.45 m. Although the height of the vines ranges between 2.0 and 2.5 m, the plant biomass is concentrated in the upper third of the canopy. The rows are oriented east-west with an inter-row spacing between the trellises is 3.35 m. This inter-row space is planted with a grass cover crop to regulate soil moisture early in the growing season following the winter season when this region receives virtually all of it rainfall. The cover crop enters senescence in mid-March and is mowed in late April or early May. As a result, the cover crop is inactive during the period considered in this study.

Other management practices shared by the two vineyards include the timing and amount of drip irrigation, pruning activities, and application of agrochemicals.

The primary difference between the two vineyards is the age of the vines. The vines at the northern vineyard (Site 1) were more mature having been planted in 2005 while the southern vineyard (Site 2) was planted in 2009. The northern vineyard, which has an area of 35 ha, is also somewhat larger than the southern vineyard; the latter has an area of 21 ha.

Data Collection and Post-Processing

The measurements of near-surface wind profiles, surface fluxes, meteorological conditions used in this study were collected using identical instrument packages. The wind velocity profiles were collected using four sonic anemometers (CSAT3[1], Campbell Scientific, Logan, Utah) mounted facing due west (270°) at 2.5 m, 3.75 m, 5 m and 8.0 m agl, respectively. The turbulent energy fluxes were determined via the eddy covariance method using a sonic anemometer (CSAT3, Campbell Scientific, Logan, Utah) to measure the orthogonal wind velocity components and an infrared gas analyzer (EC-150, Campbell Scientific) to measure the water vapor and carbon dioxide concentrations. Both sensors were mounted at 5 m agl facing due west and operated using a sampling frequency of 20 Hz. The net radiation was determined from measurements collected via a four-component radiometer (CNR-1, Kipp and Zonen, Delft, Netherlands) mounted 6 m agl. The soil heat flux was calculated as the average of 5 heat flux plates (HFT-3, Radiation Energy Balance Systems, Bellevue, Washington) deployed at a depth 8 cm along a diagonal transect across the inter-row space. A pair of thermocouples, which were buried at depths of 2 cm and 6 cm, and a soil moisture sensor (HydraProbe, Stevens Water Monitoring System, Portland, Oregon), which was buried at a depth of 5 cm, was co-located with each heat flux plate. Additional auxiliary measurements were collected using a combined

[1] The use of trade, firm, or corporation names in this article is for the information and convenience of the reader. Such use does not constitute official endorsement or approval by the US Department of Agriculture or the Agricultural Research Service of any product or service to the exclusion of others that may be suitable

humidity and temperature sensor (HMP45C, Vaisala, Helsinki, Finland) mounted 5 m agl, two thermal infrared thermometers (SI-111, Campbell Scientific) mounted 2.5 m agl at a 45° to the surface, and a tipping bucket rain gauge (TE525, Texas Electronics, Dallas, Texas),

The high-frequency (20 Hz) wind velocity data collected as a part of the wind profiles were post-processed by first screening the raw data to identify and remove without replacement nonphysical values and data spikes following the method of Goring and Nikora (2002). Then, the coordinate system of the wind velocity components was rotated to align with prevailing wind direction (Tanner and Thurtell, 1969; Kaimal and Finnigan, 1994). Finally, the hourly mean wind speed and direction was calculated.

Similarly, the flux data were post-processed using the full suite of standard corrections and adjustments. Nonphysical values and data spikes were removed without replacement from the high frequency data and a two-dimensional coordinate rotation was applied to the wind velocity data following the same procedures as used with the wind profiles. Also, the sonic temperature was converted to air temperature by adjusting for humidity effects following the approach described by Liu et al. (2001). Third, the data were corrected for sensor displacement and frequency response attenuation according to the methods outlined by Massman (2000) and Massman and Lee (2002). Finally, hourly turbulent fluxes were calculated. The moisture and carbon dioxide fluxes were then corrected for the effects of buoyancy and water vapor density (Webb et al., 1980).

Leaf Area Index

The leaf area index was estimated from satellite imagery for each year during the GRAPEX project using the reference-based technique of Gao et al. (2012). The technique uses the relationship between the LAI of homogenous MODIS pixels (500 m resolution) and the surface reflectance of the corresponding Landsat pixels to develop a regression tree. The resulting regression tree was then applied to the Landsat imagery to generate a LAI map at 30-m spatial resolution. The LAI map was smoothed and gap-filled to generate daily LAI using the Savitzky-Golay filter approach (Jonsson and Eklundh 2004). Since the experimental sites locate in the overlapped area of two adjacent Landsat paths, over 60 clear Landsat 7 and 8 images were acquired each year from 2013 to 2016. The resulting LAI curves agreed with in-situ observation to within 5% to 10%, on average. Details of the procedure and resulting LAI product used in this study are provided in Sun et al (2017).

Two-Source Energy Balance Model Description

The two-source energy balance model (TSEB), which was originally developed by Norman et al. (1995) and Kustas and Norman (1997, 1999, 2000), uses radiometric surface temperature (T_r) to determine the surface energy fluxes while explicitly considering the separate contributions of the soil and canopy. More specifically, the model uses T_r, meteorological data such as wind speed (U), and vegetation characteristics such as leaf area index (LAI) to simultaneously solve a family of equations describing the energy fluxes from the soil and canopy. Although a detailed description of the model can found elsewhere, e.g. Kustas and Norman (2000) and Kustas et al. (2012), a brief overview is provided here.

To begin, TSEB defines the T_r as the area-weighted average of the temperatures of the canopy and soil surface:

$$T_r(\phi) = \{f_c(\phi)T_c^4 + [1 - f_c(\phi)]T_s^4\}^{1/4} \quad (1)$$

where $T_r(\phi)$ is the radiometric surface temperature as a function of view angle ϕ, $f_c(\phi)$ is the fractional vegetation cover as a function of ϕ, T_c is the canopy temperature, and T_s is the soil surface temperature. The fractional vegetation cover is derived from LAI according to:

$$f_c(\phi) = 1 - \mathrm{EXP}\left(-\frac{\Omega \mathrm{LAI}}{2Cos\phi}\right) \quad (2)$$

where **Ω** is a dimensionless clumping index, which indicates the degree heterogeneity in the spatial distribution of the leaf area (Anderson et al., 2005) and the other terms are defined above.

Additionally, TSEB defines the energy budgets of the soil surface and canopy, respectively, as follows:

$$R_{Ns} = H_s + \lambda E_s + G \quad (3a)$$

$$R_{Nc} = H_c + \lambda E_c \quad (3b)$$

where R_N is the net radiation, H is the sensible heat flux, and λE is the latent heat flux. The subscript *s* refers to the soil surface while the subscript *c* refers the canopy.

The net radiation for the soil and canopy are determined using a simplified radiation transfer model (Kustas and Norman 2000) while G is computed following a modification of the method described by Santanello and Friedl (2003). Rather than using the sinusoidal function given by Santanello and Friedl (2003) to describe the relationship between G and R_n over time, a double asymmetric sigmoid function was used because it better fit the observed relationship at the study site (Nieto et al., this issue, a). That work showed the ratio of G to R_n varied from a minimum of -0.5 near sunrise/sunset to maximum near 0.35 at mid-day.

For the soil surface and canopy, respectively, H is calculated according to:

$$H_s = \rho C_p \frac{T_s - T_{ac}}{r_s} \quad (4a)$$

$$H_c = \rho C_p \frac{T_c - T_{ac}}{r_x} \quad (4b)$$

where ρ is the air density, C_p is the specific heat of air, T_{ac} is the within-canopy air temperature, r_s is the resistance of the soil surface to heat exchange, r_x is the resistance of the total canopy to heat exchange, and the other terms are defined above. In turn, λE_s is calculated as a residual while λE_c is calculated according to:

$$\lambda E_c = \alpha f_c \frac{\Delta}{\Delta+\gamma} R_{Nc} \quad (5)$$

where α is the Priestley-Taylor coefficient (Priestley and Taylor 1972) which has an initial value of 1.26, Δ is the slope of the saturation vapor pressure-temperature curve, γ is the psychrometric constant, and the other terms are defined above.

The resistance of the soil surface to heat exchange (r_s) was estimated based on a modified form of the empirical approach of Sauer et al. (1995) developed by Kustas and Norman (2000):

$$r_s = \left[a(T_s - T_{ac})^{1/3} + bU_s\right]^{-1} \quad (6)$$

where both a (0.0025 m K^{-1} s^{-1}) and b (0.012) are constants, U_s is the wind speed just above the soil surface where the effects of soil roughness is minimal, and the other terms are defined above. In turn, U_s is calculated according to Goudriann (1977):

$$U_s = U_c EXP\left[-0.28 \sqrt[3]{\frac{\mathrm{LAI}^2 h_c}{\ell}}\left(1 - \frac{1}{20h_c}\right)\right] \quad (7)$$

where U_c is the wind speed at the top of the canopy, h_c is the canopy height, ℓ is the mean leaf size, and the other terms are defined above. Similarly, U_c calculated according to Goudriann (1977) as follows:

$$U_c = U\left[\frac{ln\left(\frac{h_c - d_o}{z_o}\right)}{ln\left(\frac{z - d_o}{z_o}\right) - \Psi}\right] \quad (8)$$

where U is the wind speed at height z above the canopy, d_o is the displacement height, z_o is the roughness length for momentum, Ψ is the correction for atmospheric stability, and the other terms are defined above. Finally, as described by Norman et al. (1995), r_x is defined as:

$$r_x = \frac{c\sqrt{\ell / U_d}}{\mathrm{LAI}} \quad (9)$$

where c (90 $s^{1/2}$ m^{-1}) is a constant and U_d is determined analogously to U_s as:

$$U_d = U_c EXP\left[-0.28 \sqrt[3]{\frac{\mathrm{LAI}^2 h_c}{\ell}}\left(1 - \frac{z_o + d_o}{h_c}\right)\right] \tag{10}$$

and the other terms are defined above.

For the standard version of the TSEB model ($TSEB_{STD}$), the roughness parameters, d_o and z_o are estimated using the well-known empirical functions of h_c given by Norman and Campbell (1980), among others:

$$d_o = \frac{2}{3} h_c \tag{11a}$$

$$z_o = \frac{h_c}{8} \tag{11b}$$

For this study, h_c of the vineyard that was used by the TSEB model was estimated as a function of LAI (see Nieto et al., this issue, b). Using a typical vines height of 2.25 m for the GRAPEX field sites, these relationships estimate d_o and z_o as 1.50 m and 0.28 m, respectively.

Numerous studies, such as Shaw and Pereira (1982), has demonstrated that the roughness length is influenced by other factors beyond h_c; this is particularly true of sparse open canopies. Thus, due to the configurations of vineyards, the standard approach for estimating the roughness parameters may not be the most appropriate. Therefore, an alternate version of the TSEB model ($TSEB_{OPN}$) was also used in this study. This version of the model uses the approach of Schaudt and Dickinson (2000) to estimate the roughness parameters. The approach builds on the earlier work of Raupach (1992) and Lindroth (1993) to consider canopy shape and density, in addition to h_c, when estimating d_o and z_o.

The method of Schaudt and Dickinson (2000) begins with the assumption that the vegetation height of woody vegetation changes little over time. Instead, the roughness changes in response to changes in vegetation density, i.e. LAI, and the frontal area of the vegetation. The frontal area is the projected area of the canopy perpendicular to the wind direction of that intercept and interacts with the air flow; it is a function of the canopy height, width, and shape (Raupach 1992, 1994). From this Raupach (1994) proposed the frontal leaf area index (λ_c) defined as:

$$\lambda_c = f_c \frac{h_c}{w_c} \tag{12}$$

where f_c is the fractional canopy cover, w_c is the canopy width, and the other terms are defined as above. He further proposed the following relations for d_o and z_o as a function of λ_c:

$$d_o = h_c \left[1 - \frac{1-e^{-(a\lambda_c)^{1/2}}}{(a\lambda_c)^{1/2}}\right] \tag{13a}$$

$$z_o = \begin{cases} h_c \left[b_1 \lambda_c^{c_1} e^{-d\lambda_c^{e_1}} + f_1\right] & \lambda_c \leq 0.152 \\ h_c \left[b_2 \lambda_c^{c_2} \left(1 - e^{-d\lambda_c^{e_2}}\right) + f_2\right] & \lambda_c > 0.152 \end{cases} \tag{13b}$$

where a (15.0), b_1 (5.86), b_2 (0.0537), c_1 (1.33), c_2 (-0.51), d (10.9), e_1 (1.12), e_2 (0.874), f_1 (8.6 ×10^{-4}), and f_2 (3.68 ×10^{-3}) are coefficients and the other terms are defined as above. Finally, using the Schaudt and Dickinson (2000) approach, the roughness parameters used by the model are calculated as the product of these initial estimates and a correction factor. The correction factor for d_o and z_o, respectively, are:

$$f_d = 1 - ae^{-b\text{LAI}} \tag{14a}$$

$$f_z = \begin{cases} c_1 \text{LAI}^{3/2} + d_1 & \text{LAI} \leq 0.8875 \\ c_2 e^{-d_2\text{LAI}} + 1 & \text{LAI} > 0.8875 \end{cases} \tag{14b}$$

where a (0.3991), b (-0.1779), c_1 (0.3299), c_2 (1.6771, d_1 (2.1713), and d_2 (0.1717) are coefficients and the other terms are defined as above.

Finally, a version of the TSEB model ($TSEB_{VIN}$) that uses the relationships developed by this study was also used herein to evaluate the impact of the roughness parameterization on the modeled fluxes.

Calculation of Roughness Parameters

Using the data collected during the 2014 to 2016 growing seasons as a part of the GRAPEX project, d_o and z_o were calculated assuming a logarithmic wind profile and neutral atmospheric stability conditions. Under these conditions, the wind speed can be expressed as a function of height:

$$U = \frac{u_*}{k} ln\left(\frac{z-d_o}{z_o}\right) \tag{15}$$

where u_* is the friction velocity, k is the von karmann constant, and the other terms are defined above (Stull, 1988; Arya, 2001). Based on this relation, the d_o can be determined using paired measurements of wind speed taken at two different heights as follows:

$$d_o = z_1 - \frac{\Delta z}{e^{k\Delta U/u_*-1}} \tag{16}$$

where z_1 is the lower measurement height, Δz is the separation distance between the two measurements, ΔU is the difference in the measured wind speed, and the other terms are defined above. Once d_o is determined, z_o can be calculated by rearranging Eq. (15):

$$z_o = \frac{z-d_o}{e^{kU/u_*}} \tag{17}$$

This approach, and particularly the determination of d_o, is highly sensitive to any errors in the measurements and any violations of the underlying assumptions (Brutsaert, 1982). For example, a preliminary sensitivity analysis for the GRAPEX study sites indicates a 5% error in ΔU results in a 5% to 15% error in the calculated d_o, depending on the measurement heights used. Therefore, the data used were restricted to clear-sky days with near-neutral stability and sufficient turbulent mixing (See Table 1 for a complete listing of constraints).

For each vineyard and time period identified as valid, all possible measurement height combinations – for the purpose of this study, the wind speed measurements from the eddy covariance system were also included as a part of the profile - were used to estimate d_o following Eq. (16). As a further quality control step, the six estimates of d_o were compared. If they agreed to within 10%, d_o during the period was taken as the average of all of the d_o estimates. If there was disagreement among the estimates of d_o, the period was neglected in the subsequent analysis of d_o. Due to the constraints placed on the calculation of d_o, there were only a small number of d_o values obtained for each vineyard each year (see below for additional information). As a result, the mean d_o value (1.40 m) was used in the subsequent calculation of z_o.

The roughness length was calculated in a similar manner. For each vineyard, the valid periods conforming to the constraints listed in Table1 were first identified. Then z_o was estimated for each measurement height in the profile using Eq. (17). Again, as a further quality control step, the four estimates of z_o for each period were compared and only if they agreed to within 10% was the average used for subsequent analyses.

Table 1 The conditions used to constrain the data used to calculate the displacement height and roughness length are listed.

<table>
<tr><th>Condition</th><th>Constraint for
Displacement Height</th><th>Constraint for
Roughness Length</th></tr>
<tr><td>Incident Solar Radiation ($K_\downarrow$)</td><td colspan="2">$K_\downarrow \geq 100$ W m^{-2}</td></tr>
<tr><td>Wind Speed (U)</td><td colspan="2">$U \geq 1$ m s^{-1}</td></tr>
<tr><td>Wind Direction (φ)</td><td colspan="2">$\lvert \varphi$ -270°$\rvert \leq 90°$</td></tr>
<tr><td>Friction Velocity (u_*)</td><td colspan="2">$u_* \geq 0.1$ m s^{-1}</td></tr>
<tr><td>Atmospheric Stability (ζ)</td><td>$-0.02 \leq \zeta \leq 0.01$</td><td>$-0.04 \leq \zeta \leq 0.02$</td></tr>
</table>

The constraints used for determining the valid periods for calculating z_o are relaxed somewhat compared to those used for estimating d_o. Specifically, the range of near-neutral conditions was extended slightly. Calculations of d_o are substantially more sensitive to departures from neutral conditions than the determination of z_o. By using a u_* (0.31 m s^{-1}) typical of the sites and the stability corrections given by Paulson (1970) and Dyer (1974), the percent error of the estimates of the roughness parameters was calculated as a function of atmospheric stability. To account for the effects of atmospheric stability, Eq. (16) and Eq. 17 were modified to include the stability correction; respectively, for d_o and z_o, the modified relationships are:

$$ {}^{c}d_o = z_1 - \frac{\Delta z}{e^{k\Delta U/u_* + \Delta\psi - 1}} \tag{18a}$$

$$ {}^{c}z_o = \frac{z - d_o}{e^{kU/u_* + \psi}} \tag{18b}$$

where ${}^{c}d_o$ and ${}^{c}z_o$ are the estimates of d_o and z_o under non-neutral conditions, ψ is the stability correction, and the other terms are defined as above. The percent error is then defined as:

$$ \epsilon_{pct} = 100 \frac{|{}^{n}x - {}^{c}x|}{{}^{c}x} \tag{19}$$

where ϵ_{pct} is the percent error, ${}^{n}x$ is the estimate of the quantity of interest – either d_o and z_o – assuming neutral conditions, and ${}^{c}x$ is the estimate of the quantity of interest calculated according to Eq. (18).

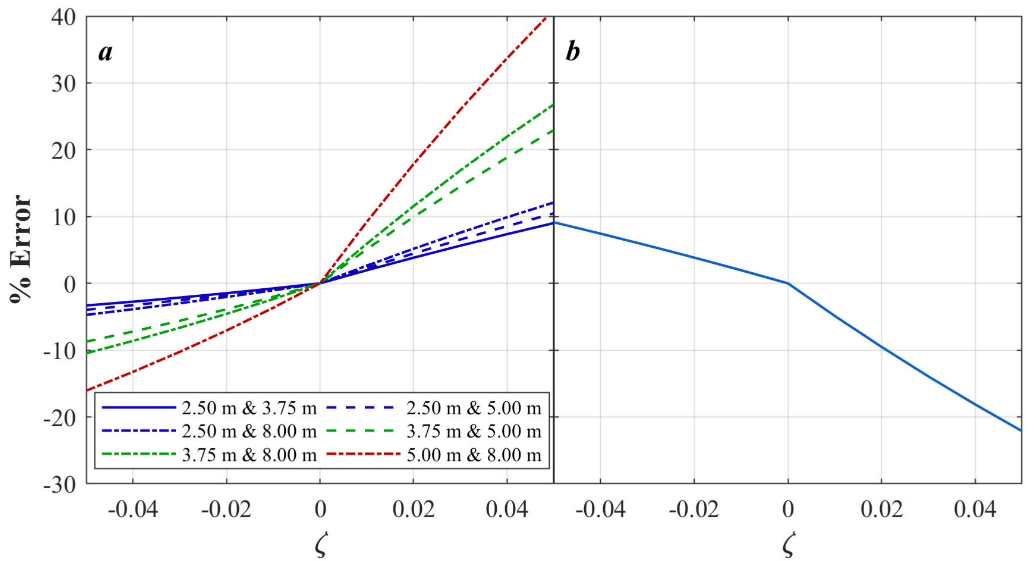

Figure 2 The percent error of the estimates of ***a***) displacement height and ***b***) roughness length as a function of atmospheric stability.

As can be seen in Figure 2, the percent error introduced into the estimates of z_o by non-neutral conditions is approximately half that introduced into the estimates of d_o. Thus, the range of ζ allowed when estimating z_o can be extended to -0.04 and 0.02 while introducing less than 10% error. While the impact of atmospheric stability on the estimates of d_o varies as a function of the measurement heights used, this is the same maximum error as was allowed for the estimates of d_o.

Statistical Analysis

A pair of well-established statistics were used to evaluate the model output of both the standard and modified TSEB model. The first is the root mean square difference (RMSD) which is defined as:

$$\text{RMSD} = \sqrt{\frac{1}{n}\sum_{i=1}^{n}(x_i - y_i)^2} \qquad (20)$$

where *x* and *y* are two estimates of some quantity of interest, *n* is the number of paired data points, and *i* is an index. The RMSD can be separated into random and systemic and components according to:

$$\mathrm{RMSD}_R = \sqrt{\frac{1}{n}\sum_{i=1}^{n}(y_i - p_i)^2} \tag{21a}$$

$$\mathrm{RMSD}_S = \sqrt{\frac{1}{n}\sum_{i=1}^{n}(p_i - x_i)^2} \tag{21b}$$

where *p* is the value predicted by ordinary least-squares regression of *y* against *x* and the remaining terms are defined above (Willmott 1982; Alfieri et al. 2011).

Since the squared difference terms in the RMSD tends to overemphasize the effects of large differences (Legates and McCabe, 1999; Willmott and Matsuura, 2005; Willmott et al., 2012), the mean absolute difference (MAD) was also used. This second metric is defined as:

$$\mathrm{MAD} = \frac{1}{n}\sum_{i=1}^{n}|x_i - y_i| \tag{22}$$

where the terms are defined as above. Note that if x and y are the actual (observed) and modeled flux, respectively, then RMSD and MAD, are indicative of the model error. The two metrics are equivalent to the root mean square error (RMSE) and mean absolute error (MAE).

RESULTS AND DISCUSSION

Estimates of the Displacement Height

After using the criteria in Table 1 to parse the data collected during the growing seasons from 2014 to 2016 over Vineyard 1, a total of 52 valid periods were identified. During the same timeframe only 10 valid periods were identified at Vineyard 2. While the valid periods identified over the two site differ in terms of wind speed, wind direction, and LAI, they all represent periods when *H* was near zero and the atmospheric stability was very close to neutral. The difference in the number of near-neutral periods at the two sites is likely due to differences in vegetation density. During the growing season, the LAI of Vineyard 2 was approximately 0.25 m^2 m^{-2} or 10% to 25% less than the LAI at Vineyard 1. Because of the lower LAI, the amount of transpiration is reduced while the surface temperature is increased at Vineyard 2. Both of these effects act to increase *H* and, thereby, unstable atmospheric conditions over Vineyard 2. A comparison of the daytime *H* and atmospheric stability (ζ) collected at each vineyard during the growing season further supports this hypothesis. Over the 4 years of GRAPEX, the daytime *H* at Vineyard 2 averaged 144 W m^{-2} or approximately 30 W m^{-2} greater than the mean at Vineyard 1. Similarly, for the same timeframe, ζ, which is the ratio of measurement height to Obukhov length, was 0.09 lower at Vineyard 2 compared to Vineyard 1.

It. was not possible to determine the relationship between d_o and site characteristics, such as LAI, because only a limited range of environmental conditions are represented by the data due to the small number of valid periods, along with their tendency to be clustered in time. As an

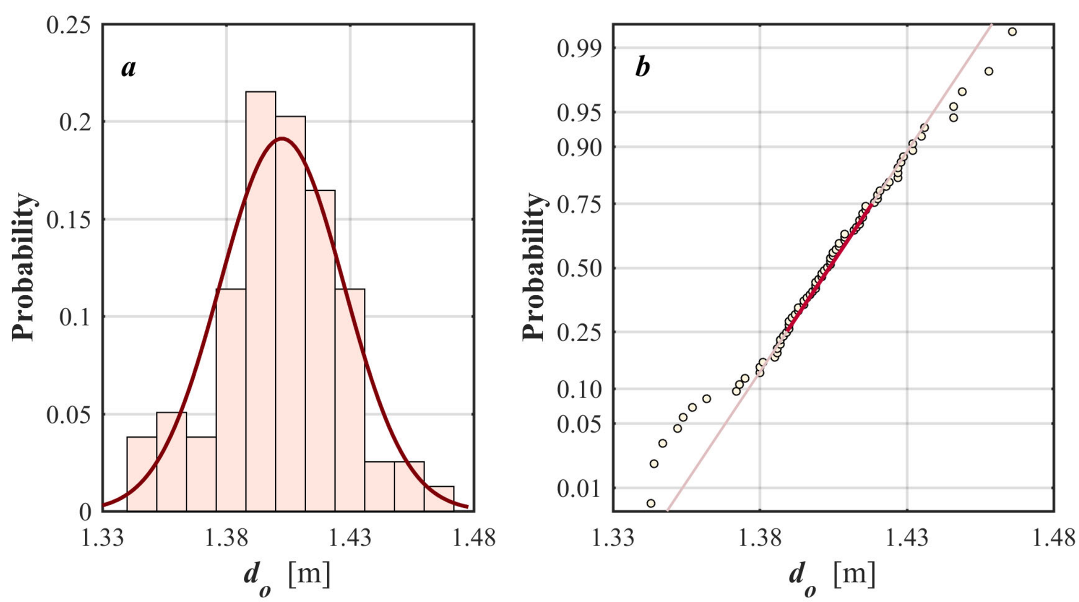

Figure 3 The ***a***) histogram overlaid with corresponding probability density function and ***b***) probability plot for the pooled estimates of the displacement height show that the quantity is normally distributed.

example of the clustering, half of the valid periods identified at Vineyard 1 during 2015 occurred on either 9 or 10-June. However, by pooling the data over both sites and all years, it was found that the estimates of d_o calculated for the valid periods, which ranged between 1.34 m and 1.47 m, were normally distributed and averaged 1.40 m with a standard deviation of 0.03 m (Fig.3). The mean d_o estimate is very near the center of the vine biomass which is approximately1.45 m, the height where the vines are attached to the trellis. This agrees with the definition of d_o as the mean height of momentum absorption by a rough surface (Raupach 1992, 1994). The mean value of d_o was used for both the calculation of z_o and the model simulations.

Estimates of the Roughness Length

After relaxing the constraints, between 36 and 40 valid periods were identified each year at Vineyard 1 while between 8 and 28 valid periods were identified for Vineyard 2 (Table 2). To investigate the relationship between z_o and LAI, the data from each year at Vineyard 1 was bin-averaged based on the corresponding LAI. The same was done for the data collected at Vineyard 2 for 2014 and 2016, the 2 years when sufficient valid periods were identified at this site. However, no relationship was evident. This is likely due to relatively small range of LAI represented by the periods identified as valid. An example using the data collect at Vineyard 1 during 2015 is shown in Figure 4represented by the periods identified as valid. An example using the data collect at Vineyard 1 during 2015 is shown in Figure 4.

Table 2 Summary statistics for roughness length for each study site and year.

Statistic	Year		
	2014	**2015**	**2016**
Vineyard 1			
n	40	34	40
Mean	0.244	0.242	0.237
Standard Deviation	0.067	0.042	0.065
Vineyard 2			
n	26	8	28
Mean	0.226	0.183	0.232
Standard Deviation	0.049	0.041	0.056

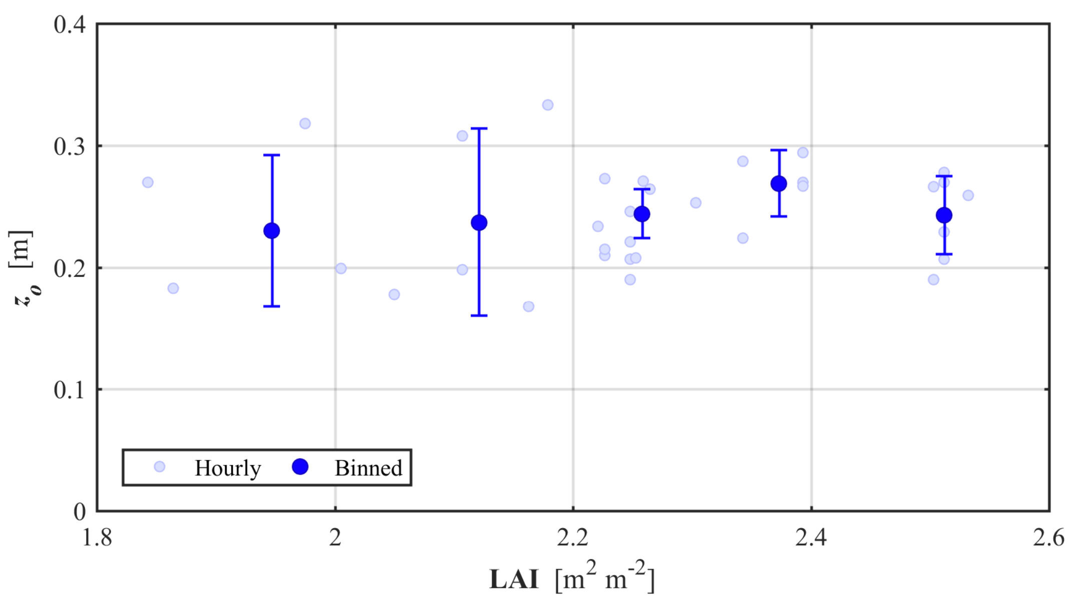

Figure 4 A plot of the roughness length (z_o) as a function of leaf area index (LAI) using the data collected at Vineyard 1 during 2015 showing the lack of a relationship between the two quantities. The error bars indicate ± 1 standard deviation.

The same procedure was used to identify the potential linkage between z_o and the wind direction relative to the row orientation. The relative wind direction (ω) is defined as 0° when the wind direction was parallel to the row direction, i.e. east to west, and 90° when the wind direction was perpendicular to the row. In this case, clear sigmoidal relationships were identified (Fig. 5) with the minimum z_o occurring when the winds were parallel to the row. These relationships can be expressed mathematically as:

$$z_o = \xi_{min} + \frac{\xi_{max} - \xi_{min}}{1 + e^{-\beta(\omega - w_o)}} \quad (23)$$

w here ξ_{min}, ξ_{max}, β, ω_o are fitting coefficients representing the minimum z_o, maximum z_o, slope, and offset in ω, respectively. Overall, with an average percent error of less than 1.5%, these relationships reproduced the observed z_o quite well; the MAE ranges between 0.002 m and 0.008 m while the RMSD ranges between 0.002 m and 0.014 m (Table 3).

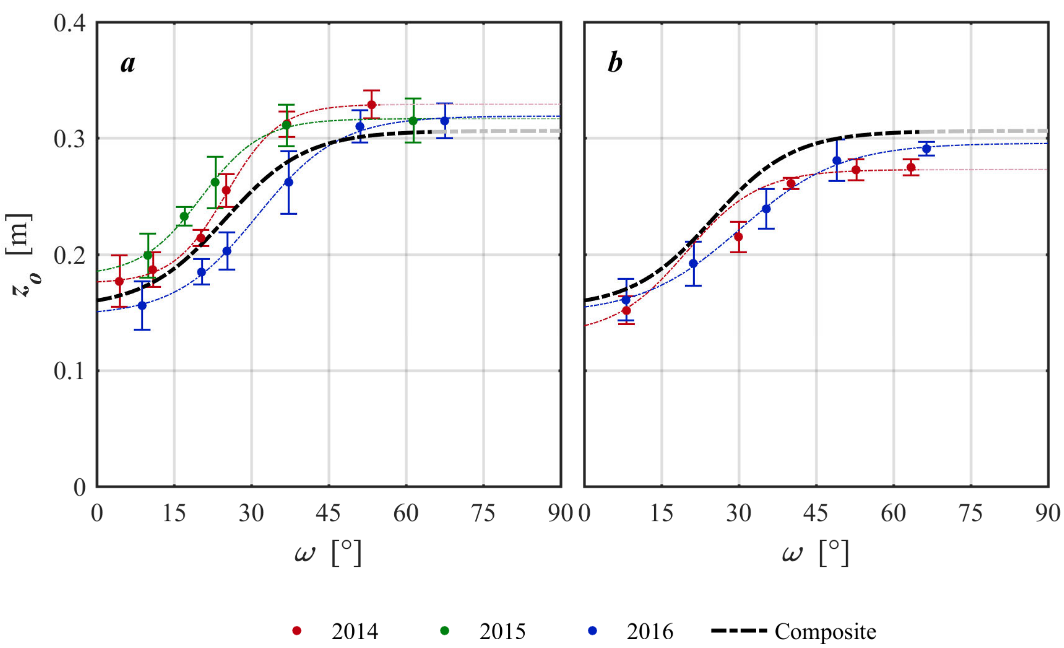

Figure 5 The best-fit sigmoidal relationships between roughness length (zo) and relative wind direction (ω) is shown for ***a***) Vineyard 1 and ***b***) Vineyard 2. The error bars indicate ± 1 standard deviation. The composite curve was determined by fitting all data from Vineyard 1 and 2.

Nonetheless, the relationships are unique both vineyard-to-vineyard and year-to-year. These variations are likely due to modest differences vine management practices that influence the amount and distribution of vine biomass, thus effective roughness of the surface. For example, pruning was more aggressive at Vineyard 1 in 2015 compared to other years. As a result, there were fewer vine shoots intruding into the inter-row space where they can interact with the wind flow. In turn, this decreases the effective roughness of the surface, particularly when ω is parallel to the rows. Similarly, the lower biomass in Vineyard 2 – as discussed above, the LAI of Vineyard 2 is approximately 0.25 m^2 m^{-2} lower than the LAI at Vineyard 1 – implies there is less vegetation, i.e. roughness elements, for the vegetation to interact with and, therefore, a lower z_o.

For the modeling purposes, a single composite relationship between z_o and ω was developed. The resulting function has the same sigmoidal form as the curves for the individual year with values of 0.1642, 0.3107, 0.1270, and 24.52 for ξ_{min}, ξ_{max}, β, and ω_o respectively (Fig. 5). While

Table 3 The error in the estimates of the roughness length when using the best-fit relationship with relative wind direction is summarized in terms of both the mean absolute difference (MAD) and root mean square difference (RMSD). The root mean square error is also partitioned between the random and systemic components.

	Vineyard 1			**Vineyard 2**	
Year	**2014**	**2015**	**2016**	**2014**	**2016**
Individual Years					
MAD	0.002	0.002	0.002	0.008	0.002
RMSD	0.003	0.002	0.002	0.014	0.002
$RMSD_R$	0.003	0.002	0.002	0.012	0.002
$RMSD_S$	0.000	0.001	0.000	0.008	0.001
Composite					
MAD	0.012	0.021	0.022	0.035	0.027
RMSD	0.015	0.023	0.025	0.036	0.028
$RMSD_R$	0.005	0.009	0.009	0.006	0.009
$RMSD_S$	0.015	0.021	0.024	0.035	0.027

the error, which averaged 8.3%, is greater than that seen for the individual years, it still suggests reasonable agreement. Not unexpectedly, the preponderance of the error is due to systemic bias when the composite relationship is used to determine z_o. For example, the composite relationship systematically overestimates z_o by approximately 0.039 m at Vineyard 2 during 2016. More generally, the effect of the systemic bias can be most easily seen through the decomposition of the RMSD (Table 3). For the best-fit relationships determined for individual years, between 72% and 100% of the error can be attributed to random error. If Vineyard 2 is neglected during 2014, this range is between 95% and 100%. In contrast when the composite relationship is used, only between 3% and 12% of the total error can be attributed to random error while between 88% and 97% of the error is systemic in nature.

Overview of the Model Intercomparison

To investigate the impact of the roughness parameterization on the modeled fluxes of heat and moisture, the output from three variants of the TSEB model were compared. The first version of the model ($TSEB_{STD}$) uses the standard parameterization estimating the roughness parameters as a fraction of h_c. The second version ($TSEB_{OPN}$) also considers the canopy geometry and vegetation density following the approach of Schaudt and Dickinson (2000). The final version ($TSEB_{VIN}$) uses the mean d_o estimated from the observations and the relationship between z_o and ω derived from the observational data. All other components of the three versions of the TSEB model are the same. The models were run over both vineyards for the years 2014 to 2016. The comparative analysis focused on daytime non-advective periods during May through August each year. Herein, daytime is defined here as period when the incident solar radiation exceeded 100 W m^{-2}. Since the onset of local advection typically occurred in mid-afternoon, the analysis considered the period nominally from 0700 to 1500 each day. This period includes stable to unstable atmospheric conditions.

Model Intercomparison of the Roughness Parameters

As can be seen in Figure 6, the different versions of the TSEB model yielded very different estimates of d_o. For all years and both vineyards, the d_o estimates from $TSTEB_{STD}$ typically ranged between 1.35 m and 1.55 m and averaged 1.46 m. Overall, the typical range of the d_o estimates from $TSEB_{OPN}$, which averaged 0.96 m, was between 0.84 m and 1.07 m. In turn, the overall MAD between the d_o estimates from $TSEB_{VIN}$ and those from $TSEB_{STD}$ and $TSEB_{OPN}$ were 0.08 m and 0.44 m, respectively. Equivalently, the estimates from $TSEB_{VIN}$ were 6% lower than $TSEB_{STD}$, on average; at the same time, they were 46% greater than the d_o estimates from $TSEB_{OPN}$. If the individual vineyards are considered, the estimates of d_o from the $TSEB_{STD}$ and $TSEB_{OPN}$ are slightly lower at Vineyard 2 compared to Vineyard 1. In both cases, the difference is approximately 0.05 m and is due to the lower LAI at Vineyard 2.

The roughness length calculated by $TSEB_{VIN}$ was typically less than z_o calculated by either $TSEB_{STD}$ or $TSEB_{OPN}$ (Fig. 7). The estimates of z_o from $TSEB_{STD}$, which typically ranged between 0.26 m and 0.30 m, varied by approximately 7% about their mean of 0.28 m. while the estimates calculated by $TSEB_{OPN}$, which typically ranged between 0.47 m and 0.49 m and averaged 0.48 m, varied by 2% about their mean. The estimates of z_o determined by $TSEB_{VIN}$ ranged between 0.17 m and 0.31 m and averaged 0.23 m. As a result, the difference in the estimates of z_o from $TSEB_{STD}$ and $TSEB_{VIN}$ in terms of MAD was 0.06 m or, equivalently 21%. More strikingly, the difference in the estimates from $TSEB_{OPN}$ and $TSEB_{VIN}$ was 0.25 m or nearly 53%. Again, there is no evident seasonal trend in the discrepancy in the estimates. This is not unexpected since the variability in the z_o calculated by $TSEB_{VIN}$ is linked to wind direction which changes on much shorter time scales. The variability in the wind direction for the hourly measurements, was typically between 5° and 30°.

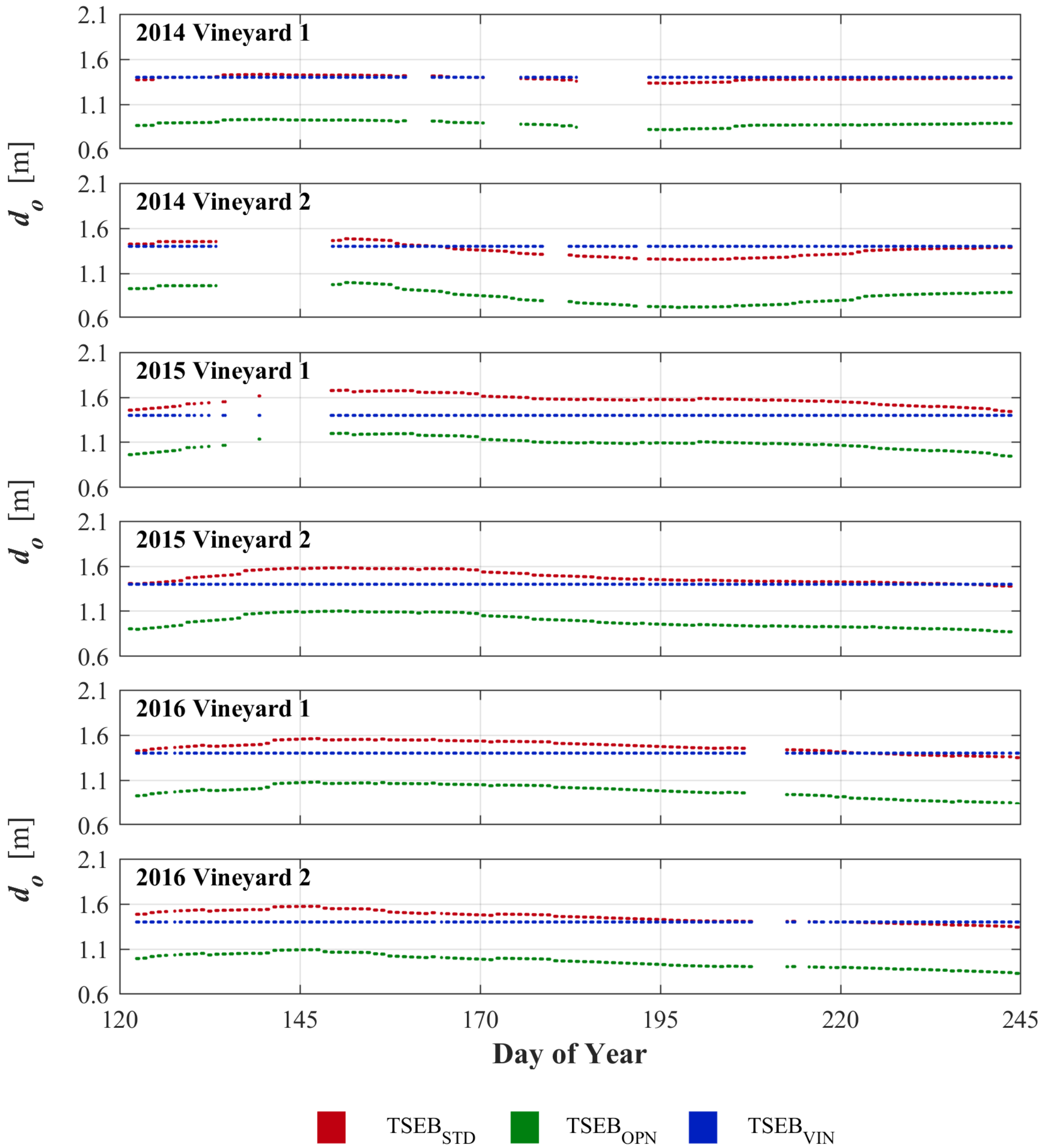

Figure 6 The estimates of displacement height from each version of the TSEB model are shown.

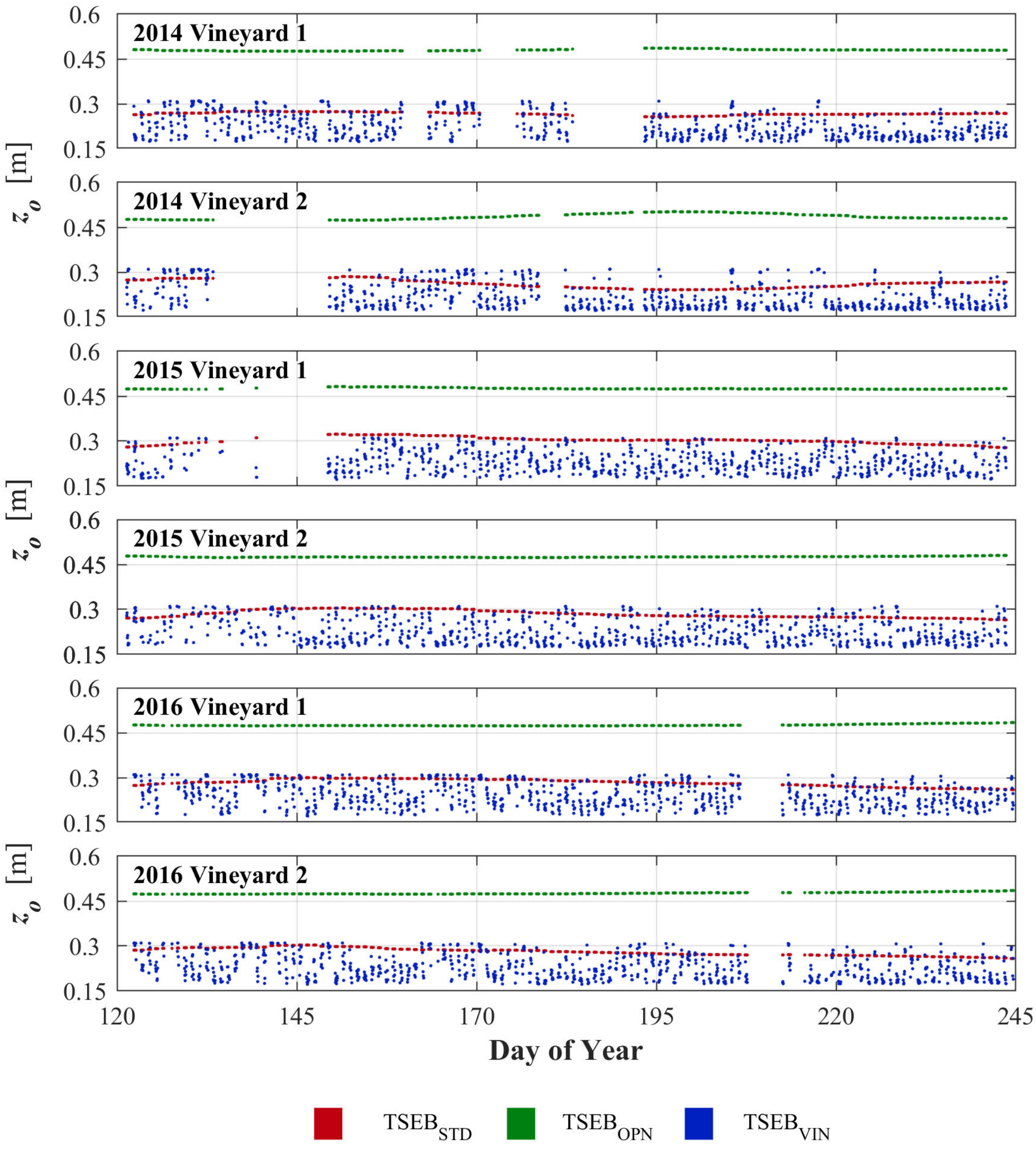

Figure 7 The estimates of roughness length from each version of the TSEB model are shown.

Model Intercomparison of the Turbulent Fluxes

The intercomparison of the model output showed consistent, albeit modest, differences in the turbulent fluxes, H and λE. Moreover, since the available energy calculated by all versions of the TSEB model is the same, the difference in one flux is counterbalance by a commensurate but opposite difference in the other. In other words, any increase (decrease) in H (λE) is balanced by a decrease (increase) in λE (H) of equal magnitude. Also, the fluxes from the canopy are unchanged by changes in the roughness parameters. This is due to the linkage between r_x and T_c in the TSEB model physics; because the quantity r_x is used in the calculation T_c, any change in r_x results in compensatory change in T_c such that, all else being equal, the models yields the same turbulent fluxes. Therefore, the changes in the turbulent fluxes due to changes in the roughness parameters are the result in changes in the fluxes from the soil only.

Given that any change in H results in an equivalent change in λE and canopy flux is unchanged by changes in the roughness parameters, the focus of this analysis is on the soil and total H. Superficially, with seasonal values of MAD and RMSD ranging from slightly more than 1.4 W m^{-2} to 3.1 W m^{-2} and 1.7 W m^{-2} to 4.0 W m^{-2}, respectively, the difference in H calculated by TSEB$_{STD}$ and TSEB$_{VIN}$ appears trivial. This is equivalent to an average decrease in H_s and H_{tot} calculated by TSEB$_{VIN}$ of 1.5% and nearly 3%, respectively. For the sake of comparison, the increases in both λE_s and λE_{tot} were less than 1%. Additionally, by partitioning the RMSD, it was found that approximately 87% of the difference can be attributed to systemic differences in the modelled fluxes.

On an hourly timescale, however, the difference between TSEB$_{STD}$ and TSEB$_{VIN}$ can be as much as 12 W m^{-2} or 7% and 13% and 7% for H_s and H_{tot}, respectively. As can be seen in Figure 8, the largest differences occur near mid-day when the available energy is greatest. It can also be seen that the differenced were more mixed; although the fraction varies somewhat with time of day, on average, the flux from $TSEB_{VIN}$ exceeded $TSEB_{STD}$ for approximately 18% of the observational periods. This is particularly evident for Vineyard 2 where the magnitude of differences tended to be larger and more varied. For a given time of day, the range of differences in the fluxes from $TSEB_{STD}$ and $TSEB_{VIN}$ was typically near 14 W m^{-2} at Vineyard 2 but only 9 W m^{-2} at Vineyard 1. Finally, it can be seen that the peak difference occurred about an hour later in the day at Vineyard 2 compared to Vineyard 1. While the cause of the differences between the two vineyards is unclear, it is hypothesized that they due to differences in vegetation density and canopy geometry. They may also reflect the effect of using a composite function to estimate z_o which compared to the individual observed relationships tended to underestimate z_o for Vineyard 1 while overestimating it for Vineyard 2.

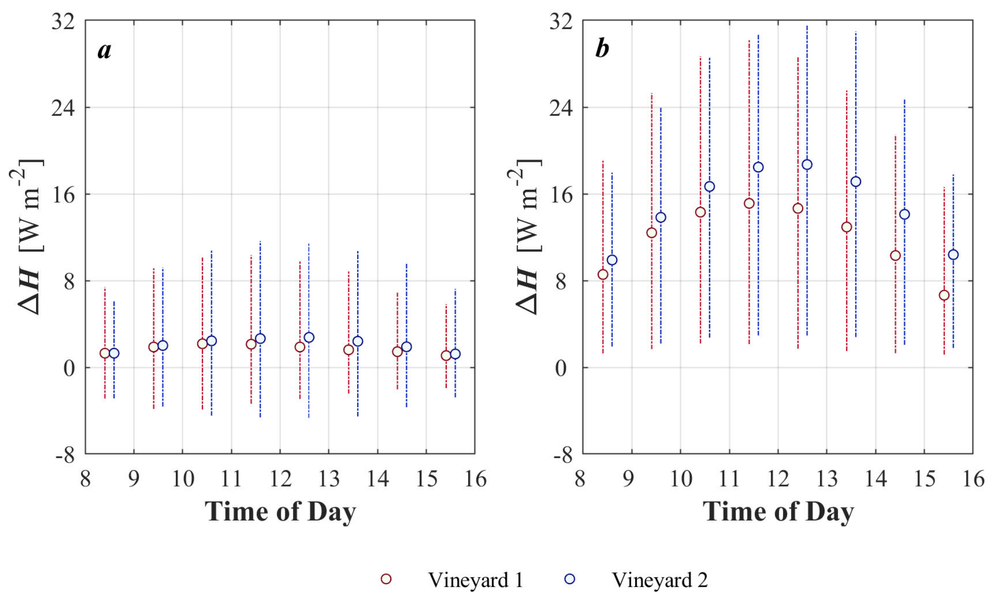

Figure 8 The mean difference of the modeled sensible heat flux calculated by ***a***) $TSEB_{STD}$ and $TSEB_{VIN}$ and ***b***) $TSEB_{OPN}$ and $TSEB_{VIN}$ is shown for each vineyard as a function of the time of day. The bars indicate the range of differences observed during each hourly period. Note, the data from each vineyard is staggered slightly in time to improve clarity.

Similarly, H_s and H_{tot} calculated by TSEB$_{VIN}$ was modestly lower than the flux calculated by TSEB$_{OPN}$. On average, the seasonal MAD was 13 W m^{-2} and RMSD was 14 W m^{-2}. This is equivalent to decrease in H_s and H_{tot} of approximately 17% and 10%, respectively. However, when considered on an hourly basis, the difference in the modeled fluxes could be as large as 32.0 W m^{-2} or, equivalently, 18% of H_{tot} and 10% of λE_{tot}. While the estimates of H_s, thus H_{tot}, from TSEB$_{OPN}$ is always greater than TSEB$_{VIN}$ during the daytime period, the same vineyard-to-vineyard differences are apparent for the fluxes output by TSEB$_{VIN}$ and TSEB$_{OPN}$. In this case, the range of differences in the modeled fluxes averaged 21 W m^{-2} at Vineyard 1 and 24 W m^{-2} at Vineyard 2. Additionally, the hourly MAD and RMSD at Vineyard 2 averaged 15 W m^{-2} and 17.0 W m^{-2}, respectively, compared to 12 W m^{-2} and 13 W m^{-2}, respectively, at Vineyard 1. Again, this indicates that the difference in the flux estimates are more varied at Vineyard 2. Finally, it can be seen in Figure 8 that the again peak difference occurred about an hour later in the day at Vineyard 2 compared to Vineyard 1.

Given the change in the roughness parameters, especially between TSEB$_{OPN}$ and TSEB$_{VIN}$, the relatively small change in the turbulent fluxes might appear counterintuitive. While d_o calculated by TSEB$_{OPN}$ was, on average, 46% less than d_o calculated by TSEB$_{VIN}$ and z_o calculated by TSEB$_{OPN}$ was, on average, 53% greater than that calculated by TSEB$_{VIN}$, H_{tot} changed by only 10%. The limited sensitivity of the TSEB model to the roughness parameters can be understood by recognizing that these quantities are primarily used to calculate the canopy level and sub-canopy wind speed terms used the TSEB model to determine r_s and ultimately H_s and H_{tot} (See Eq. 6 through 8 above). In the case of TSEB$_{OPN}$ and TSEB$_{VIN}$, the roughness parameters move in opposite directions; in other words, d_o is greater while z_o is lower for TSEB$_{VIN}$ compared to TSEB$_{OPN}$. As a result, the changes in the roughness parameters partially compensate for one another when calculating the logarithmic quantities in the relationship for U_c (Eq. 8). The sensitivity of the calculation of U_c to changes in the roughness parameters is further reduced because the logarithmic quantities change more slowly than their arguments. Moreover, while the wind speed just above the soil surface (U_s) changes proportionally with U_c, the rate of change is lower because the exponential term in Eq. 7 must be between 0 and 1; for this study that quantity ranged between approximately 0.70 and 0.75.

CONCLUSIONS AND FUTURE WORK

The results of this study demonstrate that z_o varies as a function of ω in open and highly structured canopies such as vineyard. Specifically, a clear sigmoidal relationship was found linking z_o to ω for the two vineyards considered in this study. It also showed that the relationship was unique for a given vineyard and year. This suggests that other factors, such as the vegetation density and vine management practices, also influence z_o. However, further study is needed to identify the specific factors and quantify their role in controlling z_o. It is also needed to further refine the relationships found in this study.

The work also showed that incorporating the methods for estimating the roughness parameter developed in this study into the TSEB model results significant changes in the modeled d_o and z_o. The displacement height used by $TSEB_{VIN}$ was 1.40 m or 0.06 m less than the average do from $TSEB_{STD}$ and 0.44 m greater than the average do from $TSEB_{OPN}$. The effect on z_o was more pronounce. Averaging 0.23 m, $TSEB_{VIN}$ typically produced the lowest estimates of z_o, while $TSEB_{OPN}$ produced the highest estimates; these averaged 0.48 m. The average z_o from $TSEB_{STD}$ was 0.28 m. Although the differences in the roughness parameters could be large, the did not impact the fluxes from the canopy and had only a modest effect on the fluxes from the soil. Although the difference in flux estimates from $TSEB_{STD}$ and $TSEB_{VIN}$ could be nearly 12 W

m^{-2} at midday, MAD averaged approximately 2 W m^{-2} with $TSEB_{VIN}$ partitioning slightly less energy in H_s, thus H_{tot}, compared to $TSEB_{STD}$. Similarly, the difference in the flux from $TSEB_{OPN}$ and $TSEB_{VIN}$ approached 32 W m^{-2} at midday but, on average, MAD was 13 W m^{-2}. Again, H_s and H_{tot} calculated by $TSEB_{VIN}$ was lower than that calculated by $TSEB_{OPN}$.

The results suggest that the TSEB model is largely insensitive to changes in the roughness parameters. Because of this, along with the need for additional inputs that may not be readily available and the site-specific nature of the relationship used to calculate z_o, the utility of this approach may be limited for applications using the TSEB model. Given there is no clear advantage to using the modified versions of the TSEB model, it is recommended that $TSEB_{STD}$ is used to model the fluxes over vineyards. Nonetheless, the approach may prove beneficial when used with the TSEB model over other structured canopies such as orchards. It may also prove valuable for improving other land surface models that are more sensitive to the roughness parameters (e.g., Timmermans et al., 2007; Zhan et al., 1996); these potential uses of relationships between environmental conditions and roughness deserve further evaluation.

ACKNOWLEDGMENTS

The authors would like to thank the many researchers within the USDA and other governmental agencies, university collaborators, and industry partners who have contributed to the GRAPEX project. Specifically, the authors would like to thank E.&J. Gallo Winery for financial and logistical support and the staff of Viticulture, Chemistry, and Enology Division of E.&J. Gallo Winery for their assistance with data collection. The authors would also like to thank Mr. Ernie Dosio of Pacific Agri Lands Management and the vineyard staff at the Borden/ McMannis Vineyard for their cooperation and support of this research. Finally, the authors would like to acknowledge financial support for this research from NASA [NNH16ZDA001N-WATER]. USDA is an equal opportunity provider and employer.

CONFLICT OF INTEREST

On behalf of all authors, there is no conflict of interest.

REFERENCES

Acevedo-Opazo C, Ortega-Farias S, Fuentes S (2010) Effects of grapevine (Vitis vinifera L.) water status on water consumption, vegetative growth and grape quality: An irrigation scheduling application to achieve regulated deficit. Agric Water Manage 97: 956-964.

Alfieri JG, Kustas WP, Prueger JH, Hipps LE, Chavez JL, French AN, Evett SR (2011) Intercomparison of nine meteorological stations during the BEAREX08 field campaign. J Atmos Oceanic Tech 28: 1390-1406.

Anderson MC, Norman JM, Diak GR, Kustas WP, Mecikalski JR (1997).A two-source time-integrated model for estimating surface fluxes using thermal infrared remote sensing. Remote Sens Environ 60: 195-216.

Anderson MC, Norman JM, Mecikalski JR, Torn RD, Kustas, WP, Basara, JB (2004) A multi-scale remote sensing model for disaggregating regional flues to micrometeorological scales. J Hydrometeorol 5: 343-363.

Anderson MC, Norman JM, Kustas WP, Li F, Prueger JH, Mecikalski JR (2007) A climatological study of evapotranspiration and moisture stress across the continental United States: 1. Model formulation. J Geophys Res 112: doi:10.1029/2006JD007506.

Arno J, Martınez-Casanovas J, Ribes-Dasi M, Rosell JR (2009) Review. Precision viticulture. Research topics, challenges and opportunities in site-specific vineyard management. Spanish J Agric Res 7:779–790.

Anderson MC, Norman JM, Kustas WP, Li F, Prueger JH, Mecikalski JM (2005) Effects of vegetation clumping on two-source model estimates of surface energy fluxes from an agricultural landscape during SMACEX. J Hydrometeorol 6: 892-909.

Arya P (2001) Introduction to micrometeorology. Academic Press, San Diego.

Baluja J, Diago MP, Balda P, Zorer R, Meggio, F, Morales F, Tardaguila, J (2012) Assessment of vineyard water status variability by thermal and multispectral imagery using an unmanned aerial vehicle (UAV). Irrig Sci 30: 511-522.

Bellvert J, Marsal J, Girona J, Zarco-Tejada PJ (2015). Seasonal evolution of crop water stress index in grapevine varieties determined with high-resolution remote sensing thermal imagery. Irrig Sci 33: 81-93.

Brunet Y, Finnigan JJ, Raupach MR (1994) A wind tunnel study of air flow in waving wheat: single-point velocity statistics. Boundary-Layer Meteorol 70:95–132

Brutsaert, W (1982) Evaporation into the atmosphere. D Reidel Publishing Company, Dordrecht.

California Department of Food and Agriculture (2017) California grape acreage report 2016. Available online at: http://www.nass.usda.gov/ca. Accessed 21 April 2018.

Campbell GS, Norman JM (1998), An introduction to environmental biophysics, Springer-Verlag, New York.

Campos I, Neale CMU, Calera A, Balbontin, C, Gonzalez-Piqueras J (2010) Assessing satellite-based basal crop coefficients for irrigated grapes (Vitis vinifera L.). Agric Water Manage 98: 45-54.

Chahine A, Dupont S, Sinfort C, Brunet Y (2014) Wind flow dynamics over a vineyard. Bound-Layer Meteorol 151: 557-577.

Chapman DM, Roby G, Ebeler SE, Guinard JX, Matthews MA (2005) Sensory attributes of Cabernet Sauvignon wines made from vines with different water status. Aust J Grape Wine Res 11: 339–347.

Chaves MM, Santos TP, Souza CR, Ortun˜o MF, Rodrigues ML, Lopes CM, Maroco JP, Pereira JS (2007) Deficit irrigation in grapevine improves water-use efficiency while controlling vigour and production quality. Ann Appl Biol 150:237–252.

Dyer AJ (1974) A review of flux profile relationships. Bound-Layer Meteorol, 7: 363-372.

Gao F, Anderson MC, Kustas WP, Wang Y (2012) A simple method for retrieving Leaf Area Index from Landsat using MODIS LAI products as reference. J. Appl. Remote Sens., 6, DOI: 10.1117/.JRS.1116.063554

Goring DG, Nikora VI (2002) Despiking acoustic doppler velocimeter data. J Hydrol Eng 128: 117–126.

Goudriaan, J (1977) Crop micrometeorology: A simulation study. Center for Agricultural Publications and Documentation, Wageningen.

Hicks BB (1973) Eddy fluxes over a vineyard. Agric Meteorol 12: 203-215.

John Dunham and Associates (2016) The 2015 economic impact study of the California wine industry. Available online at: http://www.wineinstitute.org/resources/statistics. Accessed 6 November 2017.

Jonsson P, Eklundh L (2004) TIMESAT—a program for analyzing time-series of satellite sensor data. Comput. Geosci. 30: 833-845.

Kaimal JC, Finnigan JJ (1994) Atmospheric boundary layer flows. Oxford University Press, Oxford.

Kustas WP, Norman JM (1997) A two-source approach for estimating turbulent fluxes using multiple angle thermal infrared observations. Water Resour Res 33: 1495-1508.

Kustas WP, Norman JM (1999) Evaluation of soil and vegetation heat flux predictions using a simple two-source model with radiometric temperatures for partial canopy cover. Agric For Meteorol 94:13-29.

Kustas WP, Norman JM (2000) A two-source energy balance approach using directional radiometric temperature observations for sparse canopy covered surfaces. Agron J 92: 847-854.

Kustas WP, Alfieri JG, Anderson MC, Colaizzi PD, Prueger JH, Evett SR, Neale CM, French AN, Hipps LE, Chávez JL, Copeland KS, Howell TA (2012) Evaluating the two-source energy balance model using local thermal and surface flux observations in a strongly advective irrigated agricultural area. Adv Water Resour 50: 120-133.

Legates DR, McCabe GR (1999) Evaluating the use of “goodness-of-fit” measures in hydrologic and hydroclimatic model validation. Water Resour Res 35: 233-241.

Lindroth A (1993) Aerodynamic and canopy resistance of short-rotation forest in relationship to leaf area index and climate. Bound-Layer Meteorol 66: 265–279.

Liu H, Peters G, Foken T (2001) New equations for sonic temperature variance and buoyancy heat flux with an omnidirectional sonic anemometer. Bound-Layer Meteorol 100: 459–468.

Lobell DB, Cahill KN, Field CB (2007) Historical effects of temperature and precipitation on California crop yields. Climatic Change 81: 187-203.

Massman WJ (2001) A simple method for estimating frequency response corrections for eddy covariance systems. Agric For Meteorol 104: 185–198.

Massman WJ, Lee X (2002) Eddy covariance flux corrections and uncertainties in long term studies of carbon and energy exchanges. Agric For Meteorol 113: 121–144.

Maurer KD, Hardiman BS, Vogel CS, Bohrer G (2013) Canopy-structure effects on surface roughness parameters: Observations in a Great Lakes mixed-deciduous forest. Agric For Meteorol 177: 24-34.

Maurer KD, Bohrer G, Kenny WT, Ivanov VY (2015) Large-eddy simulations of surface roughness parameter sensitivity to canopy-structure characteristics. Biogeosci 12: 2533-2548.

MFK Research (2007) The impact of wine, grapes, and grape products on the American economy. Available online at: https://www.wineinstitute.org/files/mfk_us_econ_report07.pdf. Accessed 6 November 2017

Nieto H, Kustas WP, Torres-Rúa A, Alfieri JG, Gao F, Anderson MC, White WA, Song L, del Mar Alsina M, Prueger JH, McKee M, Elarab M, McKee LG (2018a) Evaluation of TSEB turbulent fluxes using different methods for the retrieval of soil and canopy component temperatures from UAV thermal and multispectral imagery. Irrig Sci, this issue.

Nieto H, Kustas W, Gao F, Alfieri J, Torres A, Hipps L (2018b) Impact of different within-canopy wind attenuation formulations on modelling evapotranspiration using TSEB. Irrig Sci, this issue.

Norman JM, Kustas WP, Humes KS (1995) A two-source approach for estimating soil and vegetation energy fluxes from observations of directional radiometric surface temperature. Agric Forest Meteorol 77: 263-293.

Ojeda H, Andary C, Kraeva E, Carbonneau A, Deloire A (2002) Influence of pre and postveraison water deficit on synthesis and concentration of skin phenolic compounds during berry growth of Vitis vinifera cv. Shiraz. Am J Enol Vitic 53: 261–267.

Padro J, Massman WJ, Den Hartog G, Neumann HH (1994) Dry deposition velocity of O_3 over a vineyard obtained from models and observations: The 1991 California ozone deposition experiment. Water Air Soil Pollut 75: 307-323.

Pagay V (2016) Effects of irrigation regime on canopy water use and dry matter production of ‘Tempranillo’ grapevines in the semi-arid climate of Southern Oregon, USA. Agric Water Manage 178:271-280.

Paulson CA (1970) The mathematical representation of wind speed and temperature profiles in the unstable atmospheric boundary layer. J Appl Meteorol 9: 857-861.

Pellegrino A, Lebon E, Simonneau T, Wery J (2005) Towards a simple indicator of water stress in grapevine (Vitis vinifera L.) based on the differential sensitivities of vegetative growth components. Aust J Grape Wine Res 11: 306–315.

Pitman AJ (1994) Assessing the sensitivity of a land-surface scheme to the parameter values using a single column model. J Clim 7: 1856-1869.

Priestley CHB, Taylor RJ (1972) On the assessment of surface heat flux and evaporation using large-scale parameters. Mon Weather Rev 100: 81-92.

Raupach M (1992) Drag and drag partition on rough surfaces. Bound-Layer Meteorol 60: 375-395.

Raupach M (1994) Simplified expressions for vegetation roughness length and zero-plane displacement as functions of canopy height and area index. Bound-Layer Meteorol 71: 211-216.

Riou C, Pieri P, Valancogne C (1987) Variation de la vitesse du vent a l'interieur et au-dessus d'une vigne. Agric For Meteorol 39: 143-154.

Santanello JA, Friedl MA (2003) Diurnal variation in soil heat flux and net radiation. J Appl Meteorol 42: 851-862.

Sauer TJ, Norman JM, Tanner CB, Wilson, TB (1995) Measurement of hea and vapor transfer at the soil surface beneath a maize canopy using source plates. Agric For Meteorol 75: 161-189.

Schaudt KJ, Dickinson RE (2000) An approach to deriving roughness length and zero-plane displacement height from satellite data, prototyped with BOREAS data. Agric For Meteorol 104: 143-155.

Semmens KA, Anderson MC, Kustas WP, Gao F, Alfieri JG, McKee L, Prueger JH, Hain CR, Cammalleri C, Yang Y, Xia T, Sanchez L, Alsina MM, Velez M (2016) Monitoring daily evapotranspiration over two California vineyards using Landsat 8 in a multi-sensor data fusion approach. Remote Sens Environ 185: 155-170.

Sene KJ (1994) Parameterisations for energy transfers from a sparse vine crop. Agric For Meteorol 71: 1-18.

Shaw RH, Pereira A (1982) Aerodynamic roughness of a plant canopy: A numerical experiment. Agric Meteorol 26: 51–65.

Stull R (1988) Introduction to boundary layer meteorology. Kluwer Academic Publishers, Dordrecht

Sun L, Gao F, Anderson MC, Kustas WP, Alsina M, Sanchez L, Sams B, McKee LG, Dulaney WP, White A, Alfieri JG, Prueger JH, Melton H, Post K. (2017) Daily mapping of 30 m LAI, NDVI for grape yield prediction in California vineyard. Remote Sensing, 9, 317.

Tanner CB, Thurtell, G (1969) Anemoclinometer measurements of Reynolds stress and heat transport in the atmospheric surface layer. Research and Development Technical Report to US Army Electronic Command, ECOM 66-G22-F. Department of Soil Sciences, University of Wisconsin.

Timmermans WJ, Kustas WP, Anderson MC, French AN (2007) An intercomparison of the Surface Energy Balance Algorithm for Land (SEBAL) and the Two-Source Energy Balance (TSEB) modeling schemes. Remote Sensing of Environment. 108, 369-384.

US Department of the Treasury, Alcohol and Tobacco Tax and Trade Bureau (2017) Statistical Report – Wine. Available online at: https://www.ttb.gov/wine/wine-stats.shtml.

Verhoef A, McNaughton KG, Jacobs, AFG (1997) A parameterization of momentum roughness length and displacement height for a wide range of canopy densities. Hydrol Earth Sys Sci 1: 81-91.

Webb EK, Pearman GL, Leuning R (1980) Correction measurements for density effects due to heat and water vapour transfer. Q J Roy Meteorol Soc 106: 85–100.

Webb LB, Whetton PH, Barlow, EWR (2007) Modelled impact of future climate change on the phenology of winegrapes in Australia. Australian J Grape Wine Res 13: 165-175.

Weiss A, Allen LH (1976) Vertical and horizontal air flow above rows of a vineyard. Agric Meteorol 17: 433-452.

Willmott, CJ (1982) Some comments on the evaluation of model performance. Bull Amer Meteorol Soc, 63: 1309-1313.

Willmott C, Matsuura K (2005) Advantages of the mean absolute error (MAE) over the root mean square error (RMSE) in assessing average model performance. Climate Res 30: 79–82.

Willmott C, Robeson SM, Matsuura K (2012) A refined index of model performance. Int J Climatol 321; 2088-2094.

Xia T, Kustas WP, Anderson MC, Alfieri JG, Gao F, McKee L, Prueger JH, Geli HME, Neale CMU, Sanchez L, Alsina MM, Wang Z (2016) Mapping evapotranspiration with high-resolution aircraft imagery over vineyards using one- and two-source modeling schemes. Hydrol Earth Syst Sci 20:1523-1545.

Zarrouka O, Francisco R, Pinto-Marijuan M, Brossa R, Santos RR, Pinheiro C, Costa JM, Lopes C, Chaves MM (2012) Impact of irrigation regime on berry development and flavonoids composition in Aragonez (Syn. Tempranillo) grapevine. Agric Water Manage 114: 18-29.

Zeng X, Wang A (2007) Consistent Parameterization of Roughness Length and Displacement Height for Sparse and Dense Canopies in Land Models. J Hydrometeorol 8: 730-737.

Zhan X, Kustas WP, Humes KS (1996) An Intercomparison study on models of sensible heat flux over partial canopy surfaces with remotely sensed surface temperature. Remote Sensing of Environment. 58,242-256.